Translation from Journal of IPSJ

A Bidirectional Method for Numerical Conformal Mapping Based on the Charge Simulation Method

KANAME AMANO*

Numerical conformal mapping has been an attractive subject in numerical analysis for several decades, and is now at an exciting stage of development. Current methods fall into two groups: one for mapping a given problem domain onto a standard region, such as the unit disk, and the other for mapping in the reverse direction. No method seems to be feasible in both directions. This paper describes a bidirectional method of numerical conformal mapping between a given Jordan domain and the unit disk. The basic idea is to use the charge simulation method for solving the Dirichlet problem of Laplace's equation in order to reconstruct an approximate inverse mapping function, with the boundary correspondence established in advance. In contrast to many other methods, it does not require any nonlinear iteration procedure. It also has the following attractive features: simplicity of mathematical formulation and programming, high efficiency of computation, high accuracy of computational results, and ease of error estimation. These are demonstrated by numerical examples for some typical problem domains.

1. Introduction

Conformal mapping [1] is a fundamental subject in complex analysis with wide application in physics and engineering. However, exact mapping functions are known only for some special domains. Therefore, numerical conformal mapping has been an attractive subject in numerical analysis for several decades [2, 3], and is now at an exciting stage of development [4].

Current methods of numerical conformal mapping fall into two groups: one for mapping a given problem domain onto a standard region such as the unit disk, and the other for mapping in the reverse direction. In both cases, conformal mapping can usually be reduced to integral equations involving an unknown boundary corresponding function. However, these two groups have usually been studied independently and a bidirectional method has not yet been discovered.

In mapping from the problem domain onto the standard region, the integral equations are linear and derived from the Dirichlet problem of Laplace's equation. Symm's integral equation method [5-7] is well known, where conjugate harmonic functions are expressed by a single-layer logarithmic potential and the problem is reduced to a singular Fredholm integral equation of the first kind. Symm approximated the unknown source density with a step function, which is equivalent to the first-order derivative of the boundary corresponding function. His method was improved by Hayes, Kahaner, and Kellner [8], where a piecewise quadratic polynomial was used to approximate the source density. It was improved also by Hough and Papamichael [9, 10], where spline functions of various degrees were used and some singular functions were introduced to overcome the difficulties associated with corner singularities. $O(n^3)$ operations are needed in these methods if the boundary is discretized at n points. However, these methods are not suitable for mapping the standard region onto the problem domain.

On the other hand, in mapping from the standard region onto the problem domain, the integral equations are nonlinear and involve the conjugation operator. Theodorsen's integral equation method is well-known [11-15], where various nonlinear iterative techniques have been used. In each step of iteration, conjugate periodic functions are determined by using the fast Fourier transform, and $O(n \log n)$ operations are needed. However, these methods are not suitable for mapping the problem domain onto the standard region.

Numerical conformal mapping has been little used in scientific and engineering computation. A major difficulty for practitioners of computation may be that two different complicated algorithms are needed for mapping from the problem domain onto the standard region and for mapping in the reverse direction. Consequently, there is little software for conformal mapping.

Recently, a new method [16-18] for mapping the

This is a translation of the IPSJ 30th Anniversary Award Paper that appeared originally in Japanese in Journal of IPSJ, Vol. 31, No. 5 (1990), pp. 623-632.

*Department of Computer Science, Faculty of Engineering, Ehime University, Matsuyama 790, Japan.

given problem domain onto the standard region has been proposed, in which conjugate harmonic functions are expressed by a linear combination of logarithmic potentials. This method is based on the charge simulation method [19], which is known to be a simple and accurate solution of the Dirichlet problem of Laplace's equation, and can be easily combined with Newton's method for inverse mapping [20, 21].

This paper proposes a bidirectional method of numerical conformal mapping between a given Jordan domain and the unit disk, based on the charge simulation method. In other words, it is shown that the charge simulation method can be applied to the mappings both from the Jordan domain onto the unit disk and in the reverse direction. The basic idea is to reconstruct an approximate inverse mapping function by the same method, using the boundary correspondence established in advance. This method has the following remarkable features that distinguish it from most other methods:

(a) Numerical conformal mappings both from the problem domain onto the standard region and in the reverse direction are possible with the same algorithm.

(b) It needs no iteration procedure for mapping in the reverse direction.

Furthermore, it inherits the following attractive features from the charge simulation method: simplicity of mathematical formulation and programming, high efficiency of computation, high accuracy of computational results, and ease of error estimation. These are demonstrated by numerical examples for some typical problem domains.

2. Numerical Conformal Mapping

2.1 Riemann's Mapping Theorem

Riemann's mapping theorem tells us that a simply connected domain can be mapped conformally onto the unit disk. We are concerned here with the mapping of a Jordan domain D bounded by a Jordan curve C given in the z-plane onto the unit disk $|w|<1$ in the w-plane (Fig. 1). Taking the origin in D without loss of generality, the mapping function $w=f(z)$ is unique under the normalizing condition $f(0)=0$ and $f'(0)>0$ [3], and is expressed as

$$w=f(z)=ze^{g(z)+ih(z)}, \quad z\in D. \tag{1}$$

The functions $g(z)$ and $h(z)$ are conjugate harmonic in D and should satisfy

$$g(z)=-\log|z|, \quad z\in C \tag{2}$$

and

$$h(0)=0, \tag{3}$$

respectively from the boundary correspondence between C and $|w|=1$ and from the normalizing condition $f'(0)>0$. The condition $f(0)=0$ is obviously satisfied. The functions $\exp g(z)$ and $h(z)$ represent the extension in modulus and the rotation in argument caused by the mapping, respectively.

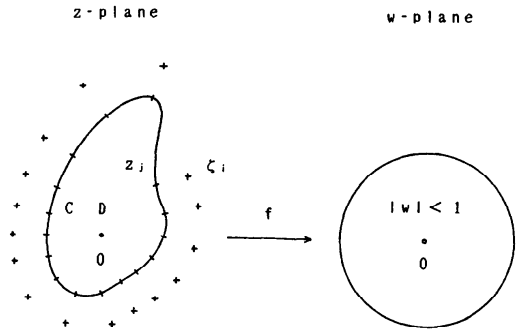

Fig. 1 Conformal mapping and the charge simulation method. The normalizing condition is $f(0)=0$ and $f'(0)>0$. ζ_i and z_j are the charge points and the collocation points, respectively.

By Carathéodory's theorem, $f(z)$ maps the closed domain $\bar{D}=D+C$ onto $|w|\leqq 1$ one-to-one continuously, including the boundary.

2.2 Charge Simulation Method

Based on the charge simulation method, the conjugate harmonic functions $g(z)$ and $h(z)$ can be approximated with a linear combination of real and imaginary parts of complex logarithmic potentials that have poles at N charge points ζ_i arranged outside the given domain D (Fig. 1). The following simple approximate mapping function

$$W=F(z)=ze^{G(z)+iH(z)}, \quad z\in\bar{D}, \tag{4}$$

$$G(z)=-\sum_{i=1}^{N} Q_i \log|z-\zeta_i|, \tag{5}$$

$$H(z)=-\sum_{i=1}^{N} Q_i \arg(z-\zeta_i)+\theta_0$$
$$=-\sum_{i=1}^{N} Q_i \arg(1-z/\zeta_i), \tag{6}$$

is then obtained [16]. Here,

$$\theta_0=\sum_{i=1}^{N} Q_i \arg(-\zeta_i) \tag{7}$$

is a constant of rotation determined by the normalizing condition (3). Capitals W, F, G, and H are approximations to w, f, g, and h, respectively. The N charges Q_i are undetermined coefficients, and can be determined to satisfy the boundary condition (2) at N collocation points z_j arranged on the boundary C. That is to say, the values of Q_i are solutions of a system of simultaneous linear equations

$$\sum_{i=1}^{N} Q_i \log|z_j-\zeta_i|=\log|z_j|, \quad z_j\in C,$$
$$j=1, 2, \cdots, N, \tag{8}$$

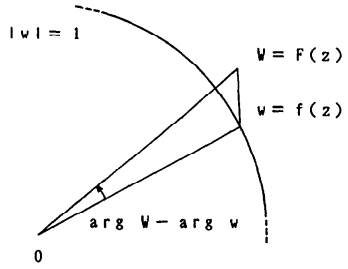

Fig. 2 Error estimation on the boundary curve using the maximum modulus theorem for regular functions.

which is called the collocation condition.

Note that the approximate mapping function $F(z)$ is regular, regardless of the discretization error in $G(z)$ and $H(z)$ and of the cancelling error in solving simultaneous linear equations.

2.3 Error Estimates

The maximum modulus theorem for regular functions can be used to estimate computational errors. Because $F(z)$ and $f(z)$ are single-valued regular in the bounded domain D and continuous on its boundary C, the absolute error of the approximate mapping function $E_W(z)$ takes its maximum value E_W on C and can be estimated (see Fig. 2) as

$$\begin{aligned} E_W(z) &\equiv |W(z)-w(z)| \equiv |F(z)-f(z)| \\ &\leqq \max_C |W(z)-w(z)| \equiv E_W \\ &\leqq \max_C \{|\,|W(z)|-|w(z)|\,| \\ &\quad + |w(z)|\,|\arg W(z)-\arg w(z)|\} \\ &= \max_C |\,|W(z)|-1\,| \\ &\quad + \max_C |\arg W(z)-\arg w(z)|. \end{aligned} \tag{9}$$

Here, $\max_C$ denotes the estimate on the boundary C. Note that the relations

$$\begin{aligned} E_M &\equiv \max_C E_M(z) \equiv \max_C |\,|W(z)|-1\,| \\ &\fallingdotseq \max_C |G(z)-g(z)| \equiv \max_C E_G(z) \equiv E_G \end{aligned} \tag{10}$$

and

$$\begin{aligned} E_A &\equiv \max_C E_A(z) \equiv \max_C |\arg W(z)-\arg w(z)| \\ &= \max_C |H(z)-h(z)| \equiv \max_C E_H(z) \equiv E_H \end{aligned} \tag{11}$$

hold. Errors of the conjugate harmonic functions $G(z)$ and $H(z)$ may be expected to be of the same order, since they are derived from the same simulation charges, and

$$E_G \fallingdotseq E_H. \tag{12}$$

In other words,

$$E_M \fallingdotseq E_A \tag{13}$$

between the errors of the modulus and argument components of the approximate mapping function $F(z)$. This conjecture has been confirmed by practical experience [16, 22]. Finally, we obtain the relation

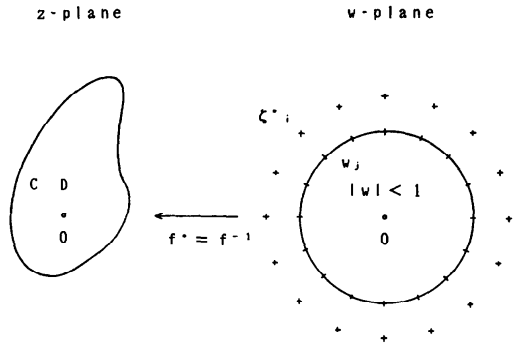

Fig. 3 Inverse conformal mapping and the charge simulation method. The normalizing condition is $f^*(0)=0$ and $f^{*\prime}(0)>0$. ζ_i^* and w_j are the charge points and the collocation points, respectively.

$$E_W(z) \leqq E_W \leqq E_M + E_A \fallingdotseq 2E_M, \tag{14}$$

which allows us to estimate errors by using only the computational results on the boundary. Furthermore, E_M can be simply estimated as

$$E_M \fallingdotseq \max_j |\,|W(z_{j+1/2})|-1\,|, \quad z_{j+1/2} \in C, \tag{15}$$

since the collocation condition (8) is equivalent to $E_M(z_j)=0$. Here, $z_{j+1/2}$ is an intermediate point on the boundary between the two collocation points z_j and z_{j+1}.

Finally, in the numerical conformal mapping based on the charge simulation method, simple error estimates are available a posteriori using only the computational results at the intermediate points on the boundary.

3. Numerical Inverse Conformal mapping

3.1 Mapping Theorem

We are concerned here with the conformal mapping of the unit disk $|w|<1$ in the w-plane onto a Jordan damain D bounded by a Jordan curve C given in the z-plane (Fig. 3). Taking the origin in D without loss of generality, the mapping function $z=f^*(w)$ is unique under the normalizing condition $f^*(0)=0$ and $f^{*\prime}(0)>0$ [3]. By Carathéodory's theorem, $f^*(w)$ maps the closed unit disk $|w| \leqq 1$ onto $\bar{D}=D+C$ one-to-one continuously, including the boundary.

This $z=f^*(w)$ is nothing but the inverse of the preceding conformal mapping $w=f(z)$, which can be shown in the following way. Since $w=f(z)$ is mapped one-to-one from $\bar{D}$ onto $|w| \leqq 1$, its inverse $z=f^{-1}(w)$ is unique and single-valued on $|w| \leqq 1$, and the inverse is regular in $|w|<1$ and

$$f^{-1\prime}(w) = 1/f'(z). \tag{16}$$

Therefore, $f^{-1}(0)=0$ and $f^{-1\prime}(0)>0$ from the normalizing condition of $f(z)$. Consequently, $f^*(w)=f^{-1}(w)$

from the uniqueness of $f^*(w)$.

We express the mapping function as

$$z=f^*(w)=we^{g^*(w)+ih^*(w)}, \quad |w|<1 \tag{17}$$

in the same way as for Equation (1). The functions $g^*(w)$ and $h^*(w)$ are conjugate harmonic in $|w|<1$ and should satisfy

$$g^*(w)=\log|z|-\log|w|, \quad |w|=1 \tag{18}$$

and

$$h^*(0)=0, \tag{19}$$

respectively from the boundary correspondence between $|w|=1$ and C and from the normalizing condition $f^{*\prime}(0)>0$. The condition $f^*(0)=0$ is obviously satisfied. Note that, for $w=f(z)$,

$$g^*(w)+g(z)=0 \tag{20}$$

and

$$h^*(w)+h(z)=0 \tag{21}$$

between the two sets of conjugate harmonic functions.

Since Equation (18) involves the unknown quantity $z=f^*(w)$ in the right side, it is difficult to determine the harmonic function $g^*(w)$ by solving the Dirichlet problem of Laplace's equation. The reason why the second term $\log|w|$ is left will be given later.

3.2 Charge Simulation Method

We approximate the mapping $z=f^*(w)$ by the approximate inverse $F^{-1}(w)$, not by the exact inverse $f^{-1}(w)$. By using the charge simulation method, this inverse $F^{-1}(w)$ can be obtained numerically in the same way as $F(z)$ itself.

First, we adopt as the collocation points in the w-plane N^* suitable points w_j such that $w_j=F(z_j)$, $z_j\in C$ (Fig. 3). Outside the unit disk $|w|\leqq 1$, we arrange N^* charge points ζ_i^* corresponding to each of the collocation points. Then, the conjugate harmonic functions $g^*(w)$ and $h^*(w)$ can be approximated with a linear combination of real and imaginary parts of complex logarithmic potentials that have poles at ζ_i^*. The following simple approximate mapping function

$$Z=F^*(w)=we^{G^*(w)+iH^*(w)}, \quad |w|\leqq 1, \tag{22}$$

$$G^*(w)=-\sum_{i=1}^{N^*} Q_i^* \log|w-\zeta_i^*|, \tag{23}$$

$$H^*(w)=-\sum_{i=1}^{N^*} Q_i^* \arg(w-\zeta_i^*)+\theta_0^* = -\sum_{i=1}^{N^*} Q_i^* \arg(1-w/\zeta_i^*) \tag{24}$$

is then obtained. Here,

$$\theta_0^*=\sum_{i=1}^{N^*} Q_i^* \arg(-\zeta_i^*) \tag{25}$$

is a constant of rotation determined by the normalizing condition (19). The N^* charges Q_i^* are undetermined coefficients, and can be determined to satisfy the boundary condition (18) at N^* collocation points w_j. That is to say, the values of Q_i^* are solutions of a system of simultaneous linear equations

$$\sum_{i=1}^{N^*} Q_i^* \log|w_j-\zeta_i^*|=\log|w_j|-\log|z_j|, \quad j=1, 2, \cdots, N^* \tag{26}$$

which is called the collocation condition. Note that $z_j=F^{-1}(w_j)$ of the second term is known for the collocation points $w_j=F(z_j)$, $z_j\in C$. The first term $\log|w_j|=\log|F(z_j)|$ is not always zero, because of errors in the approximate mapping function. This is why the second term of Equation (18) was not removed.

A simple and practical way of determining the collocation points w_j is to adopt the images of the N collocation points z_j used for the approximate mapping function $F(z)$. Then, each w_j is determined automatically from z_j, and values of w_j are specified for tracing the shape of the problem domain D if values of z_j are specified in the z-plane. Additional programming is not needed for the inverse mapping $F^*(w)$. We have only to re-call the same subprogram as used for computing $F(z)$, exchanging the input and output relations of the z- and w-planes. This is a remarkable characteristic not found in any other method of numerical conformal mapping. Equations (20) and (21) are useful for checking the validity of computation.

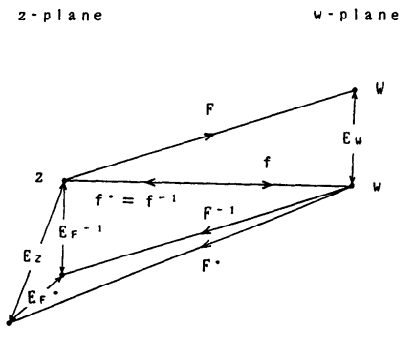

Fig. 4 Estimation of the error in numerical inverse conformal mapping.

3.3 Error Estimates

We have approximated the mapping function $f^*(w)=f^{-1}(w)$ by $F^{-1}(w)$, which has been further approximated by $F^*(w)$ according to the charge simulation method (Fig. 4). The maximum modulus theorem for regular functions can also be used to estimate errors in inverse mapping. Because $F^*(w)$ and $F^{-1}(w)$ are single-valued regular in the bounded domain $|w|<1$ and continuous on its boundary $|w|=1$, the absolute error of $F^*(w)$ with respect to $F^{-1}(w)$ takes its maximum value

on $|w|=1$ and can be estimated as

$$E_F^*(w)\equiv|F^*(w)-F^{-1}(w)|$$
$$\leqq\max_C^*|F^*(w)-F^{-1}(w)|\equiv E_F^*$$
$$\fallingdotseq\max_k|F^*(w_k)-z_k|. \tag{27}$$

The notations $\max_C^*$ and $\max_k$ denote the estimate on the unit circle $|w|=1$ and at the collocation points and the intermediate points, respectively. Similarly, for the error of $F^{-1}(w)$ with respect to $f^{-1}(w)$,

$$E_F^{-1}(w)\equiv|F^{-1}(w)-f^{-1}(w)|$$
$$\leqq\max_C^*|F^{-1}(w)-f^{-1}(w)|\equiv E_F^{-1}$$
$$\fallingdotseq\max_C\{|F(z)-f(z)|/|F'(z)|\}$$
$$\leqq E_W/\min_C|F'(z)|\equiv\tilde{E}_F^{-1}$$
$$\fallingdotseq E_W/\min_k|F'(z_k)|. \tag{28}$$

Here, in addition to the maximum modulus theorem, note that the ratio of local enlargement by mapping with a regular function is equal to the modulus of its derivative. $F'(z)\neq0$ is a necessary condition of the conformality. Consequently, for the total error of $F^*(w)$ with respect to $f^{-1}(w)$,

$$E_Z(w)\equiv|F^*(w)-f^{-1}(w)|$$
$$\leqq\max_C^*|F^*(w)-f^{-1}(w)|\equiv E_Z$$
$$\leqq\max_C^*\{|F^*(w)-F^{-1}(w)|+|F^{-1}(w)$$
$$-f^{-1}(w)|\}$$
$$\leqq E_F^*+E_F^{-1}$$
$$\lesssim E_F^*+\tilde{E}_F^{-1}\equiv\tilde{E}_Z. \tag{29}$$

Thus, simple error estimates can also be obtained by using only the computational results on the boundary in the inverse mapping. The estimates of $\tilde{E}_F^{-1}$ and $\tilde{E}_Z$ are for the worst case in which the errors of the approximate mapping function $F(z)$ and the enlargement ratio of its inverse $1/|F'(z)|$ take their maximum values at the same boundary point. Practically, the relation

$$E_Z\fallingdotseq E_F^*\ll\tilde{E}_Z \tag{30}$$

holds well in many cases, as shown later. From Equations (4)~(6),

$$F'(z)=e^{G(z)+iH(z)}\left\{1-z\sum_{i=1}^{N}Q_i/(z-\zeta_i)\right\}, \tag{31}$$

$$|F'(z)|=e^{G(z)}\left[\left\{1-\sum_{i=1}^{N}Q_i\frac{x(x-\xi_i)+y(y-\eta_i)}{|z-\zeta_i|^2}\right\}^2\right.$$
$$\left.+\left\{\sum_{i=1}^{N}Q_i\frac{x(y-\eta_i)-y(x-\xi_i)}{|z-\zeta_i|^2}\right\}^2\right]^{1/2}. \tag{32}$$

4. Numerical Examples

4.1 Collocation Points and Charge Points

In the charge simulation method, the collocation points and the charge points should be arranged according to the given domain and the boundary condition. However, optimization is difficult because of the multivariableness of the problem. Appropriateness may be empirically judged by the following qualitative criteria: high accuracy of the computational results, simplicity of the arrangement, wide applicability, and stability of the accuracy obtained.

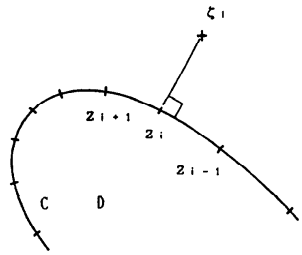

Fig. 5 Arrangement of the collocation points and the charge points in the charge simulation method.

We first arrange a suitable set of collocation points z_i, $i=1,\cdots,N$ on the boundary of the given Jordan domain so that they are generally dense in regions where the distortion is large (Fig. 5). Then, we specify the charge point ζ_i corresponding to each collocation point z_i by means of the equation

$$\zeta_i=z_i+r|z_i-z_{i-1}|e^{i\{\arg(z_i-z_{i-1})-\pi/2\}}. \tag{33}$$

Here, r is a positive parameter independent of i. As a result, the charge points are in the outward normal directions at the corresponding collocation points and dense near the boundary, where distortion is large. It is known from numerical examples that this method gives a good arrangement of points in many cases [17, 18, 20–22]. If the given domain has corners on the boundary, Equation (33) is modified as

$$\zeta_i=z_i+r/2|z_{i+1}-z_{i-1}|e^{i\{\arg(z_{i+1}-z_{i-1})-\pi/2\}} \tag{33'}$$

at the corner points. Satisfactory results can usually be obtained for $r=1\sim10$.

In inverse mapping, the collocation points w_i in the w-plane are determined to be the images of the collocation points z_i in the z-plane, as stated previously. The charge points ζ_i^* in the w-plane are also determined from Equation (33).

The conventional boundary extension method for charge arrangement [16, 19], though it has been used extensively and can give good results for near-circular domains, is not successful for flat or concave domains. Moreover, it is not applicable to non-starlike domains.

4.2 Computational Results

The notation used in the presentation of numerical results is as follows.

N: Total number of collocation points or charge points. Numbers in parentheses are for unknowns of the simultaneous linear equations to be solved when the

symmetry of the given domain is used in computation.

r_Z, r_W: Parameters of the charge arrangement in the z- and w-planes, respectively.

E_M, E_A, E_W: Errors in the numerical conformal mapping of the given Jordan domains onto the unit disk, defined by Equations (9)–(11).

E_F^*, $E_{F^{-1}}$, E_Z, $\tilde{E}_{F^{-1}}$, $\tilde{E}_Z$: Errors in the inverse mappings, that is, mapping of the unit disk onto the given Jordan domains, defined by Equations (27)–(29).

The equations used to estimate errors can be summarized as follows:

$$E_M(\fallingdotseq E_G)=\max_j |\,|F(z_{j+1/2})|-1\,|,$$

$$E_A(=E_H)=\max_k |\arg F(z_k)-\arg f(z_k)|,$$

$$E_W=\max_k |F(z_k)-f(z_k)|,$$

$$E_F^*=\max_k |F^*(w_k)-F^{-1}(w_k)|,$$

$$E_{F^{-1}}=\max_k |F^{-1}(w_k)-f^{-1}(w_k)|,$$

$$E_Z=\max_k |F^*(w_k)-f^{-1}(w_k)|,$$

$$\tilde{E}_{F^{-1}}=E_W/\min_k |F'(z_k)|,$$

$$\tilde{E}_Z=E_F^*+\tilde{E}_{F^{-1}}.$$

The subscript k denotes the estimate at the collocation points and intermediate points, as mentioned previously. The approximation $E_W\fallingdotseq 2E_M$ is used for $\tilde{E}_{F^{-1}}$ when the exact mapping function is not known.

Computations were carried out on a FACOM M-360AP machine at the Data Processing Center of Ehime University. Crout's method LAX and DLAX in SSL II were used to solve the simultaneous linear equations.

Table 1 Error estimates in the case of the circular domains $(x-x_c)^2+y^2\leqq 1$. N is the number of simulation charges, and r_Z and r_W are the parameters for their arrangement in the z- and w-planes, respectively. E denotes a computational error. Double-precision arithmetic is used in (c2).

	(a)	(b)	(c1)	(c2)
x_c	1/2	3/4	7/8	
N	33 (17)	64 (33)	64 (33)	128 (65)
r_Z	4.0	3.0	2.0	3.0
r_W	4.0	3.0	3.0	4.0
E_M	1.4E-6	1.7E-5	1.1E-3	1.2E-6
E_A	1.4E-6	3.2E-6	1.2E-3	1.2E-6
E_W	1.9E-6	1.9E-5	1.2E-3	1.2E-6
E_F^*	3.0E-6	1.0E-5	4.3E-4	1.1E-6
$E_{F^{-1}}$	2.5E-6	1.9E-5	1.8E-4	1.3E-7
E_Z	3.1E-6	1.6E-5	5.4E-4	1.2E-6
$\tilde{E}_{F^{-1}}$	5.7E-6	1.3E-4	1.8E-2	1.8E-5
$\tilde{E}_Z$	7.9E-6	1.4E-4	1.8E-2	1.9E-5

Example 1 Eccentric Circle

Problem domain $(x-x_c)^2+y^2\leqq 1$

Mapping function $w=f(z)=z/\{1+x_c(z-x_c)\}$

$z=f^{-1}(w)=(1-x_c^2)w/(1-x_c w)$

Collocation points $x_j=\cos\theta+x_c$

$y_j=\sin\theta$

$\theta=2\pi(j-1)/N$

This is an example of uniformly convex domains. The parameter $x_c(0<x_c<1)$, that is, the distance between

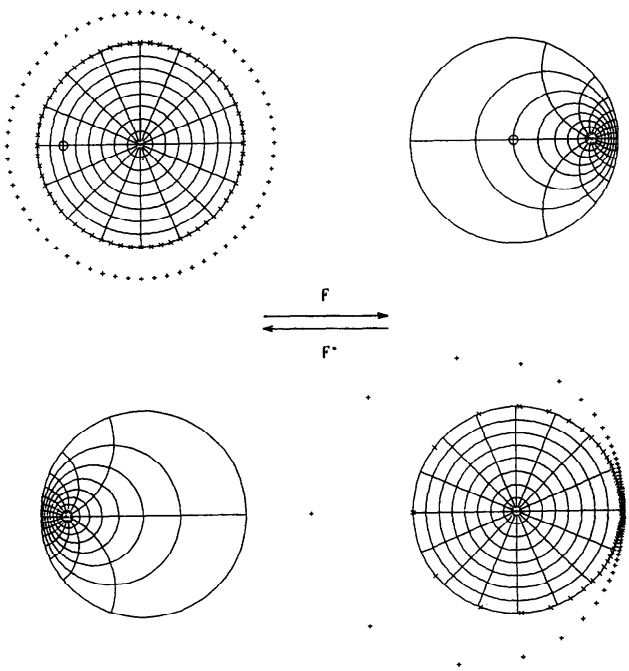

Fig. 6 Numerical conformal mapping of a circular domain and its inverse mapping by the charge simulation method.

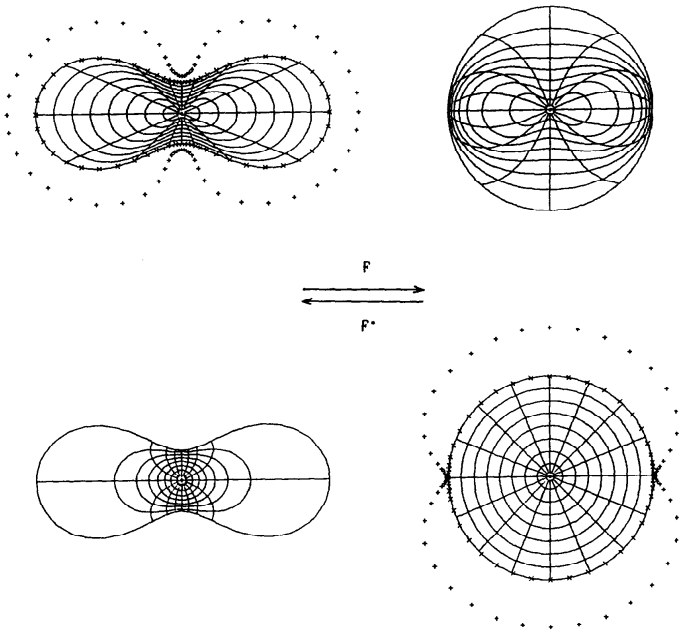

Fig. 7 Numerical conformal mapping of a Cassini's oval domain and its inverse mapping by the charge simulation method.

the normalizing point and the center of the circle controls the difficulty of the mapping problem. The collocation points are uniformly spaced along the entire boundary. The collocation points in the w-plane are the images of these collocation points in the z-plane. As mentioned previously, they are specified for tracing the shape of the given problem domain. The charge points are arranged mechanically by Equation (33) in the z- and w-planes.

Figure 6, which corresponds to Table 1(b) (but $r_W=1.5$), illustrates the mappings from the given problem domain onto the unit disk and in the reverse direction. The symbols ○, ×, and + show the normalizing point, the collocation points, and the charge points, respectively. Comparison of the computational results with the exact mapping function is possible in this example. The values of E_W and E_Z in the table show the high accuracy of bidirectional mapping. We can also see that $E_M \fallingdotseq E_A$, $E_W \leqq E_M+E_A \fallingdotseq 2E_M$ and $E_Z \fallingdotseq E_F^* \ll \tilde{E}_Z$ of Equations (13), (14), and (30) hold well. Note that the FACOM M-360AP machine has six significant hexadecimal digits in single-precision arithmetic, which corresponds to 6.3–7.2 significant decimal digits. As the normalizing points approache the boundary, the accuracy of the computational results decreases and the difference between E_F^{-1} and $\tilde{E}_F^{-1}$ or E_Z and $\tilde{E}_Z$ increases. However, as shown by (c1) and (c2), the accuracy increases sharply if N increases and double-precision arithmetic is used in computation.

The accuracy of the computational results is regular and stable with respect to the change of parameters r_Z and r_W. That is to say, the accuracy first increases and then decreases as r_Z and r_W increase, where high accuracy is obtained for a wide range of parameters.

Table 2 Error estimates in the case of Cassini's oval domains $\{(x+1)^2+y^2\}\{(x-1)^2+y^2\} \leqq a^4$. Double-precision arithmetic is used in (c2).

	(a)	(b)	(c1)	(c2)
a	$2^{1/2}$	$2^{1/16}$	$2^{1/128}$	
N	32 (9)	64 (17)	64 (17)	128 (33)
r_Z	2.5	2.0	1.0	2.5
r_W	3.0	2.5	1.5	2.5
E_M	2.8E-6	1.9E-5	2.6E-4	8.9E-7
E_A	3.6E-6	3.9E-6	2.1E-4	7.0E-7
E_W	3.7E-6	1.7E-5	2.7E-4	8.9E-7
E_F^*	5.9E-6	2.9E-5	1.9E-3	1.7E-5
E_F^{-1}	8.4E-6	3.6E-5	2.8E-3	1.9E-6
E_Z	6.3E-6	3.1E-5	3.4E-3	1.6E-5
$\tilde{E}_F^{-1}$	1.3E-5	3.0E-4	3.5E-2	1.1E-4
$\tilde{E}_Z$	1.9E-5	3.2E-4	3.7E-2	1.3E-4

Example 2 Cassini's Oval

Problem domain $\{(x+1)^2+y^2\}\{(x-1)^2+y^2\} \leqq a^4$

Mapping function $w=f(z)=az/(a^4-1+z^2)^{1/2}$

$z=f^{-1}(w)$

$=(a^4-1)^{1/2}w/(a^2-w^2)^{1/2}$

Collocation points $x_j=r\cos\theta$, $y_i=r\sin\theta$

$r=\{\cos 2\theta+(\cos^2 2\theta+a^4-1)^{1/2}\}^{1/2}$

$\theta=2\pi(j-1)/N$

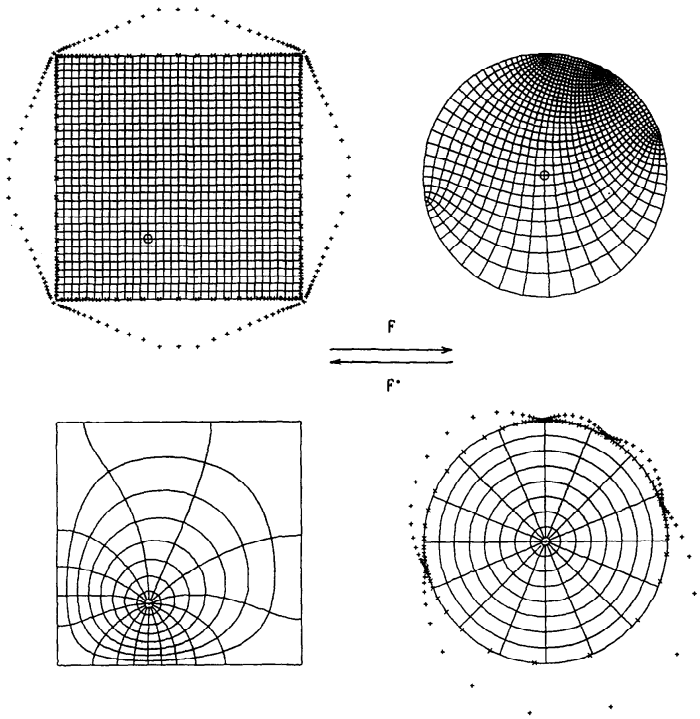

Fig. 8 Numerical conformal mapping of a square domain and its inverse mapping by the charge simulation method.

The product of the distances from the two points $(-1, 0)$ and $(1, 0)$ is less than or equal to a^2 in this domain. The parameter a controls the domain's shape and the difficulty of the mapping problem. We are interested in the case $1<a\leqq 2^{1/2}$ as an example of a concave domain. It looks like an ellipse $x^2/3+y^2=1$ when $a=2^{1/2}$, and the concavity becomes more pronounced as a decreases, until it is finally cut off at the origin when $a=1$. The collocation points are equidistant in argument along the given boundary. The other collocation points and the charge points are determined in the same manner as in the previous example.

Figure 7 corresponds to Table 2(b) ($a=1.044273$). The width of the concavity in (c) ($a=1.005430$) is about one third of that in (b). Comparison of the computational results with the exact mapping function is also possible in this example. The values of E_W and E_Z in the table show the high accuracy of the bidirectional mapping, and the error relations (13), (14), and (30) hold well. As the parameter a decreases to 1, the accuracy of the results decreases and the difference between $E_{\bar{F}^{-1}}$ and $\tilde{E}_{\bar{F}^{-1}}$ or E_Z and $\tilde{E}_Z$ increases. However, as shown by (c1) and (c2), the accuracy increases sharply if N increases in double-precision arithmetic.

The accuracy of the computational results is regular and stable with respect to the change of parameters r_Z and r_W.

Table 3 Error estimates in the case of square domains $|x-x_c|\leqq 1$ and $|y-y_c|\leqq 1$.

	(a)	(b1)	(b2)	(b3)
(x_c, y_c)	(0, 0)		(1/4, 1/2)	
N	64 (17)	64	128	256
r_c	10.0	10.0	10.0	10.0
r_Z	2.0	2.0	2.5	3.0
r_W	0.5	1.0	1.0	1.0
E_M	1.5E-4	7.0E-4	1.3E-5	6.6E-6
E_F^*	9.9E-3	1.3E-2	6.5E-3	3.0E-3
E_C	8.5E-3	1.2E-2	5.6E-3	2.6E-3

Example 3 Square

Problem domain $|x-x_c|\leqq 1, \quad |y-y_c|\leqq 1$

Colloation points $x_j=1+x_c$

$$y_j=(1-r^{j-1})/(1-r^{N/8})+y_c$$

$$r^{N/8-1}=1/r_c$$

$$j=1, \cdots, N/8+1$$

This is an example of a domain with corners on the boundary. The collocation points are arranged so that they are dense near the corners by a geometrical series with the common ratio r, which is determined by the parameter r_c. The number density near the corners is about r_c times that near the midpoints of the sides. The other collocation points and the charge points are deter-

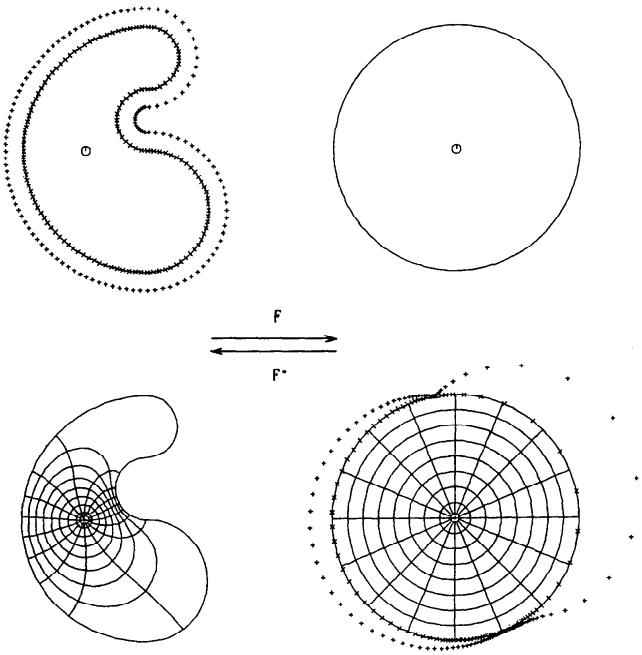

Fig. 9 Numerical conformal mapping of a comma-shaped bead domain and its inverse mapping by the charge simulation method.

mined in the same manner as in the previous examples by using Equations (33) and (33′).

Figure 8 corresponds to Table 3 (b2). Conformal mapping of the unit disk onto polygonal domains is known as the Schwarz-Christoffel transformation. The mapping functions $f(z)$ and $f^{-1}(w)$ are expressed by elliptic functions and elliptic integrals, respectively. However, they are not elementary, and we do not compare the computational results obtained with them. We focus here on the possibility of estimating errors even if the exact mapping function is not known. That is to say, the error of the numerical mapping $F(z)$ can be estimated and determined to be sufficiently small by using the error relation $E_W \lesssim 2E_M$ of Equation (14) and the computational values of E_M. On the other hand, neither E_Z nor $\tilde{E}_Z$ can be estimated in the inverse mapping, owing to the singularity at the corners where $f'(z)=0$. However, it is not difficult to estimate the gap between the image of the unit circle given by $F^*(w)$ and the original square as

$$E_C = \max_C^* (\min |F^*(w) - z_C|)$$
$$\fallingdotseq \max_k (\min |F^*(e^{i\arg w_k}) - z_C|), \quad z_C \in C. \tag{34}$$

The results show that $E_Z (\fallingdotseq E_C) \fallingdotseq E_F^*$ of Equation (30) may also hold well in this example. The accuracy increases if N increases, as shown in (b1)~(b3). However, the increase in the inverse mapping is slow, which suggests that the charge simulation method is suitable for the Dirichlet problem without singularities in the boundary condition. However, it is important that numerical mapping of the unit disk onto a square domain can be obtained simply with an accuracy of 10^{-3}.

The accuracy of the computational results is regular and stable with respect to a change in the parameter r_Z, but errors in the inverse mapping increase rapidly if the parameter r_W becomes large.

Example 4 Comma-Shaped Bead

This is an example of an asymmetric and non-starlike domain in which the whole boundary cannot seen from the normalizing point. The boundary curve is constructed by connecting four semicircles with radii 1/4, 1/4, 1, and 1/2, in this order (Fig. 9). The largest one is $(x-x_c)^2+y^2=1$, $x \leqq x_c$. The collocation points are uniformly spaced along the entire boundary. The other collocation points and the charge points are determined in the same manner as in the previous examples.

Figure 9 corresponds to Table 4(a2). Because of the non-starlikeness, it is difficult to illustrate the numerical mapping $F(z)$ by using curves similar to the boundary and radial lines from the origin. However, it is easy to image $F(z)$ from the inverse mapping.

The exact mapping function is not known, and the error E_W should be estimated from E_M in the same way as in the preceding example. The errors of the inverse mapping, $\tilde{E}_{\bar{z}^1}$ and $\tilde{E}_Z$, can be estimated in this case. However, it should be remembered that they are based on the worst situation, as stated previously. The gap be-

Table 4 Error estimates in the case of a comma-shaped bead domain.

	(a1)	(a2)	(a3)
(x_c, y_c)		(0.5, 0)	
N	64	128	256
r_Z	1.5	3.0	3.5
r_W	1.0	1.5	1.5
E_M	1.0E-3	2.4E-4	8.2E-5
E_F^*	1.5E-2	1.5E-3	7.5E-4
$\tilde{E}_F^{-1}$	7.5E-2	2.5E-2	8.6E-3
$\tilde{E}_Z$	9.0E-2	2.7E-2	9.0E-3
E_C	7.0E-3	1.1E-3	3.4E-4

tween the image of the unit circle given by $F^*(w)$ and the original comma-shaped bead shows that $E_Z(\fallingdotseq E_C) \fallingdotseq E_F^*$ of Equation (30) may hold well and that the accuracy of the inverse mapping is satisfactory.

The accuracy of the computational results increases if N increases. It is regular and stable with respect to a change in r_Z, but the errors of the inverse mapping increase more rapidly than in examples 1 and 2 if r_W becomes large.

5. Concluding Remarks

A bidirectional method of numerical conformal mapping between a given Jordan domain and the unit disk has been successfully proposed and tested on some typical domains. It has the remarkable feature that mappings both from the problem domain onto the standard region and in the reverse direction can be obtained simply without a nonlinear iteration procedure. Errors can also be estimated a posteriori by using the computational results on the boundary.

The following subjects remain for future studies:

(a) Applicability to the mapping of exterior and doubly connected domains. The fundamentals of the method may be applicable. However, its practical utility should be tested numerically.

(b) Arrangement of the collocation points and charge points. A mechanical method should be established that is independent of the given problem domain. Optimization is difficult, owing to the multivariableness of the problem. However, in the application to the conformal mapping, a practical method may be found, since the problem to be solved is determined only by the given domain and the normalizing point.

(c) Development of mathematical software. Very little software exists for conformal mapping, which could be used extensively in scientific and engineering computation. The charge simulation method may be suitable for this purpose if it is possible to arrange the collocation points and the charge points mechanically.

References

1. HENRICI, P. *Applied and Computational Complex Analysis.* **1**, John Wiley & Sons, New York, 1974.
2. GAIER, D. *Konstruktive Methoden der Konformen Abbildung.* Springer-Verlag, Berlin, 1964.
3. HENRICI, P. *Applied and Computational Complex Analysis.* **3**, John Wiley & Sons, New York, 1986.
4. TREFETHEN, L. N. ed. *Numerical Conformal Mapping.* North-Holland, Amsterdam, 1986; reprinted from *J. Comput. Appl. Math.*, **14**, 1 & 2 (1986).
5. SYMM, G. T. An Integral Equation Method in Conformal Mapping. *Num. Math.*, **9** (1966), 250–258.
6. SYMM, G. T. Numerical Mapping of Exterior Domains. *Num. Math.*, **10** (1967), 437–445.
7. SYMM, G. T. Conformal Mapping of Doubly-Connected Domains. *Num. Math.*, **13** (1969), 448–457.
8. HAYES, J. K., KAHANER, D. K. and KELLNER, R. G. An Improved Method for Numerical Conformal Mapping. *Math. Comput.*, **26**, 118 (1972), 327–334.
9. HOUGH, D. M. and PAPAMICHAEL, N. The Use of Splines and Singular Functions in an Integral Equation Method for Conformal Mapping. *Num. Math.*, **37** (1981), 133–147.
10. HOUGH, D. M. and PAPAMICHAEL, N. An Integral Equation Method for the Numerical Conformal Mapping of Interior, Exterior and Doubly-Connected Domains. *Num. Math.*, **41** (1983), 287–307.
11. HENRICI, P. Fast Fourier Methods in Computational Complex Analysis, *SIAM Rev.*, **21**, 4 (1979), 481–527.
12. GUTKNECHT, M. H. Solving Theodorsen's Integral Equation for Conformal Maps with the Fast Fourier Transform and Various Nonlinear Iterative Methods. *Num. Math.*, **36** (1981), 405–429.
13. GUTKNECHT, M. H. Numerical Experiments on Solving Theodorsen's Integral Equation for Conformal Maps with the Fast Fourier Transform and Various Nonlinear Iterative Methods. *SIAM J. Sci. Stat. Comput.*, **4**, 1 (1983), 1–30.
14. GUTKNECHT, M. H. Numerical Conformal Mapping Methods Based on Function Conjugation. *J. Comput. Appl. Math.*, **14**, 1&2 (1986), 31–77.
15. SONG, E., SUGIURA, H. and SAKURAI, T. Methods for Solving Theodorsen's Equation in Numerical Conformal Mapping. *Trans. IPS Japan*, **30**, 4 (1989) (in Japanese), 393–401.
16. AMANO, K. Numerical Conformal Mapping Based on the Charge Simulation Method. *Trans. IPS Japan*, **28**, 7 (1987) (in Japanese), 697–704.
17. AMANO, K. Numerical Conformal Mapping of Exterior Domains Based on the Charge Simulation Method. *Trans. IPS Japan*, **29**, 1 (1988) (in Japanese), 62–72.
18. AMANO, K. Numerical Conformal Mapping of Doubly-Connected Domains by the Charge Simulation Method. *Trans. IPS Japan*, **29**, 10 (1988) (in Japanese), 914–924.
19. MURASHIMA, S. *Charge Simulation Method and Its Application.* Morikita Shuppan. Tokyo, 1983 (in Japanese).
20. AMANO, K., TAKAMATSU, T. and ABE, H. Numerical Inverse Conformal Mapping by the Charge Simulation Method Combined with Newton's Method. *Trans. IPS Japan*, **30**, 4 (1989) (in Japanese), 411–418.
21. AMANO, K., TAKAMATSU, T. and ABE, H. Numerical Inverse Conformal Mapping of Exterior Domains by the Charge Simulation Method Combined with Newton's Method. *Trans. IPS Japan*, **30**, 8 (1989) (in Japanese), 923–931.
22. AMANO, K. Error Properties of Numerical Conformal Mapping Based on the Charge Simulation Method. *Trans. IPS Japan*, **32**, 1 (1991) (in Japanese), 1–10.